Quantum Rescaling, Domain Metastability, and Hybrid Domain-Walls in 2D CrI_3 Magnets

*Dina Abdul Wahab, Mathias Augustin, Samuel Manas Valero, Wenjun Kuang, Sarah Jenkins, Eugenio Coronado, Irina V. Grigorieva, Ivan J. Vera-Marun, Efrén Navarro-Moratalla, Richard F. L. Evans, Kostya S. Novoselov, and Elton J. G. Santos**

Higher-order exchange interactions and quantum effects are widely known to play an important role in describing the properties of low-dimensional magnetic compounds. Here, the recently discovered 2D van der Waals (vdW) CrI_3 is identified as a quantum non-Heisenberg material with properties far beyond an Ising magnet as initially assumed. It is found that biquadratic exchange interactions are essential to quantitatively describe the magnetism of CrI_3 but quantum rescaling corrections are required to reproduce its thermal properties. The quantum nature of the heat bath represented by discrete electron–spin and phonon–spin scattering processes induces the formation of spin fluctuations in the low-temperature regime. These fluctuations induce the formation of metastable magnetic domains evolving into a single macroscopic magnetization or even a monodomain over surface areas of a few micrometers. Such domains display hybrid characteristics of Néel and Bloch types with a narrow domain wall width in the range of 3–5 nm. Similar behavior is expected for the majority of 2D vdW magnets where higher-order exchange interactions are appreciable.

The rediscovery of magnetism in layered van der Waals (vdW) systems[1] has sparked an increasing interest in the investigation of spin interactions at the ultimate limit of few atom thick materials.[2–11] With the advent of new techniques of isolation, manipulation, measurements, and theoretical predictions, vdW magnets have become a playground for achieving the limit of magnetism in atomically thin crystals and unveil novel physical phenomena. Implementation of 2D vdW magnets in real technologies, however, requires the description of their magnetic properties through an archetypal spin model such as Ising or Heisenberg. This gives a predictive indicator to what kind of behavior is expected if such a magnet could be probed experimentally. For instance, Ising is incompatible with the appearance of magnons or spin-waves since just two spin states (e.g., $\pm z$) are taken into account.[12] If atomic spins $\mathbf{S}_i = \mu_s \mathbf{s}_i$, where μ_s is the magnetic moment, need to precess to a different spatial orientation the Heisenberg model would give unrestricted values of $\mathbf{S}_i$ on the unit sphere surface $|\mathbf{s}_i| = 1$ in order to minimize the exchange interaction energy. As dimensionality determines the stabilization of spin ordering differently to the bulk phase, previously demonstrated for many low-dimensional nanostructures,[13–15] higher-order exchange interactions beyond the Heisenberg or Ising models would be expected to play a key role in the magnetic properties of the magnetic layers. Of particular interest is CrI_3 where magnetization has been firstly measured using magneto-optical Kerr effect setup[2] at the limit of monolayer. Although CrI_3 has been treated as an Ising ferromagnet due to its large

D. A. Wahab, M. Augustin
School of Mathematics and Physics
Queen's University
Belfast BT7 1NN, UK

Dr. S. M. Valero, Prof. E. Coronado, E. Navarro-Moratalla
Instituto de Ciencia Molecular
Universidad de Valencia
Calle Catedrático José Beltrán 2, 46980 Paterna, Spain

W. Kuang, Prof. I. V. Grigorieva, Dr. I. J. Vera-Marun,
Prof. K. S. Novoselov
School of Physics
University of Manchester
Oxford Road, Manchester M13 9PL, UK

S. Jenkins, Dr. R. F. L. Evans
Department of Physics
The University of York
York YO10 5DD, UK

Prof. K. S. Novoselov
Department of Material Science & Engineering
National University of Singapore
Block EA, 9 Engineering Drive 1, 117575 Singapore

Prof. K. S. Novoselov
Chongqing 2D Materials Institute
Liangjiang New Area, Chongqing 400714, China

Dr. E. J. G. Santos
Institute for Condensed Matter Physics and Complex Systems
School of Physics and Astronomy
The University of Edinburgh
Edinburgh EH9 3FD, UK
E-mail: esantos@ed.ac.uk

The ORCID identification number(s) for the author(s) of this article can be found under https://doi.org/10.1002/adma.202004138.

DOI: 10.1002/adma.202004138

anisotropy, recent findings reporting the appearance of topological spin-excitations,[16] temperature dependent magnons,[17] and angle-dependent ferromagnetic resonance[18] indicate that the magnetic properties of CrI_3 are far beyond Ising.

Here, we show that these puzzling features can be naturally reconciled with the inclusion of biquadratic (BQ) interactions in an extended Heisenberg framework including additional quantum rescaling corrections. Our starting point is the following spin Hamiltonian:

$$H = -\sum_{ij} J_{ij}(\mathbf{S}_i \cdot \mathbf{S}_j) - \sum_{i,j} \lambda_{ij} S_i^z S_j^z - \sum_i D_i \left(S_i^z\right)^2 - \sum_{ij} K_{ij} \left(\mathbf{S}_i \cdot \mathbf{S}_j\right)^2 \quad (1)$$

where $\mathbf{S}_i$ is the localized magnetic moment unit vector on Cr atomic sites i which are coupled by pair-wise exchange interactions. J_{ij} and λ_{ij} are the isotropic and anisotropic bilinear (BL) exchanges, respectively, and D_i is the onsite magnetic anisotropy. We used up to third-nearest neighbors on both J_{ij} and λ_{ij}. The fourth term represents a biquadratic (BQ) exchange which occurs due to the hopping of more than one electron between two adjacent sites.[13,19] Its strength is given by the constant K_{ij}, which is the simplest and most natural form of non-Heisenberg coupling. We can determine K_{ij} by calculating the energetic variation of the spins $\mathbf{S}_i$ at each Cr site at different rotation angle θ including spin–orbit coupling[20–22] (**Figure 1**a). See Sections S1–S4, Supporting Information for details, and comparison with other models, such as Kitaev.[23,24] It is noteworthy that λ_{ij} and K_{ij} in monolayer CrI_3 have close magnitudes but are slightly smaller than J_{ij} (Table S1, Supporting Information). Indeed, in materials where the exchange is for some reason weak due to different processes, such as competition between ferromagnetic and antiferromagnetic exchange,[25] BQ exchange has a particularly strong influence as observed for several different compounds.[14,26–29] This seems to be the case for most of the vdW magnets as recently demonstrated.[19] We can apply similar analysis to bulk CrI_3 which shows the same magnitude of BQ exchange for the intralayer interactions but smaller for the interlayer counterparts (Table S1, Supporting Information). These results indicate that higher-order exchange processes involving two or more electrons are important in CrI_3 magnets despite of the dimensionality. Nevertheless, we focus on the effect of BQ exchange on the magnetic features of CrI_3 not considering higher order interactions, that is, three-site spin interactions.[30]

To simulate the temperature and dynamic properties of CrI_3 at a macroscopic level, we have implemented the BQ exchange interactions shown in Equation (1) within the Monte Carlo Metropolis algorithm[31] also taking into account contributions from the next-nearest neighbors. See Section S5, Supporting Information for details. In this Monte Carlo model we assume a classical spin vector $\mathbf{S}_i$ on each atomic site i of fixed length μ_s whose direction can vary freely in 3D space. The quantization vector for the spin is a local quantity which naturally includes the effects of local thermal spin fluctuations and magnon processes. This clearly separates classical and quantum contributions to the magnetic behavior of CrI_3. To analyse whether the Ising or the non-Heisenberg model (Equation (1)) provides the best description of the magnetic properties of bulk and monolayer CrI_3, we undertake a quantitative comparison between both models with the measurement of the magnetization M versus temperature T using first-principles parameters as input. We use the magneto-optical Kerr effect (MOKE) data extracted from ref. [2] for monolayer CrI_3, and the superconducting quantum interference device (SQUID) technique for bulk CrI_3 (Sections S6 and S7, Supporting Information). Figure 1a,b show the simulated temperature dependence of the magnetization of bulk and monolayer CrI_3 relative to the experimental data. It is clear that the Ising model grossly overestimates the measured Curie temperature (T_C) for both systems by several tens of Kelvins reaching high temperatures. Ising gives $T_C \approx 200$ K and $T_C \approx 102$ K for bulk and monolayer CrI_3, respectively, which is also in disagreement with previous experimental studies.[2,32–34] This suggests that a single quantization axis where spins are allowed to take only two values parallel or anti-parallel to the surface is not accurate enough to represent the magnetic properties of CrI_3 magnets. Conversely, the non-Heisenberg model gives a sound agreement with the measurements resulting in Curie temperatures of 44.4 K and 62.2 K for monolayer and bulk CrI_3, respectively. We have also checked whether other models can give a sound description of the magnetic properties of CrI_3. Namely, a Heisenberg model without the inclusion of BQ interactions,[35] a Kitaev model,[23,24] and also the BQ model in Equation (1) including non-collinear spin-textures at the level of Dzyaloshinskii–Moriya interactions (DMI). See Sections S4 and S8, Supporting Information for details. While DMI do not give any variation of T_C relative to the initial BQ model, both the Heisenberg and Kitaev models significantly underestimate the magnitude of the critical temperatures by several tens of Kelvin's relative to the measurements ($T_C^{\text{Kitaev}} = 17.2$ K, $T_C^{\text{Heisenberg}} = 23 - 37.4$ K). These results suggested that BL models are insufficient to describe the magnetic features of CrI_3. Furthermore, the inclusion of BQ exchange has recently been observed in the description[19] of neutron scattering measurements on the magnon spectra of CrI_3.[16] Even though the gap opening at the Dirac point is due to the presence of Dzyaloshinskii–Moriya interactions (DMI), the interplay between BQ exchange and DMI plays a substantial role in several features observed in the spin waves at different $\mathbf{k}$-points.[36,37] In particular at the magnon dispersion at the K–M–K path at the Brillouin zone.[19] These findings provide further background on the effect of BQ exchange on the magnetic properties of CrI_3.

The shape of $M(T)$ obtained from the classical Monte Carlo simulations instead of Equation (1) shows a much stronger curvature than displayed by the measured data at low temperatures. To better reflect the quantum nature of the heat bath of the CrI_3 systems, we apply quantum rescaling methods[38] to adjust the average strength of the thermal spin fluctuations within the non-Heisenberg model. The method has previously been applied to quantitatively describe the temperature dependent magnetization of Fe, Co, Ni, and Gd magnets. We extend the approach to monolayer and bulk CrI_3 (Figure 1c). Physically the temperature rescaling represents the quantum nature of the heat bath, consisting of discrete electron–spin and phonon–spin scattering processes. At low temperatures the spin directions are dominated by exchange interactions preferring ferromagnetic alignment of localized Cr spins. In the case of electron–spin scattering, only energetic electrons are inelastically scattered causing a local spin flip, while low energy electrons are elastically scattered and no

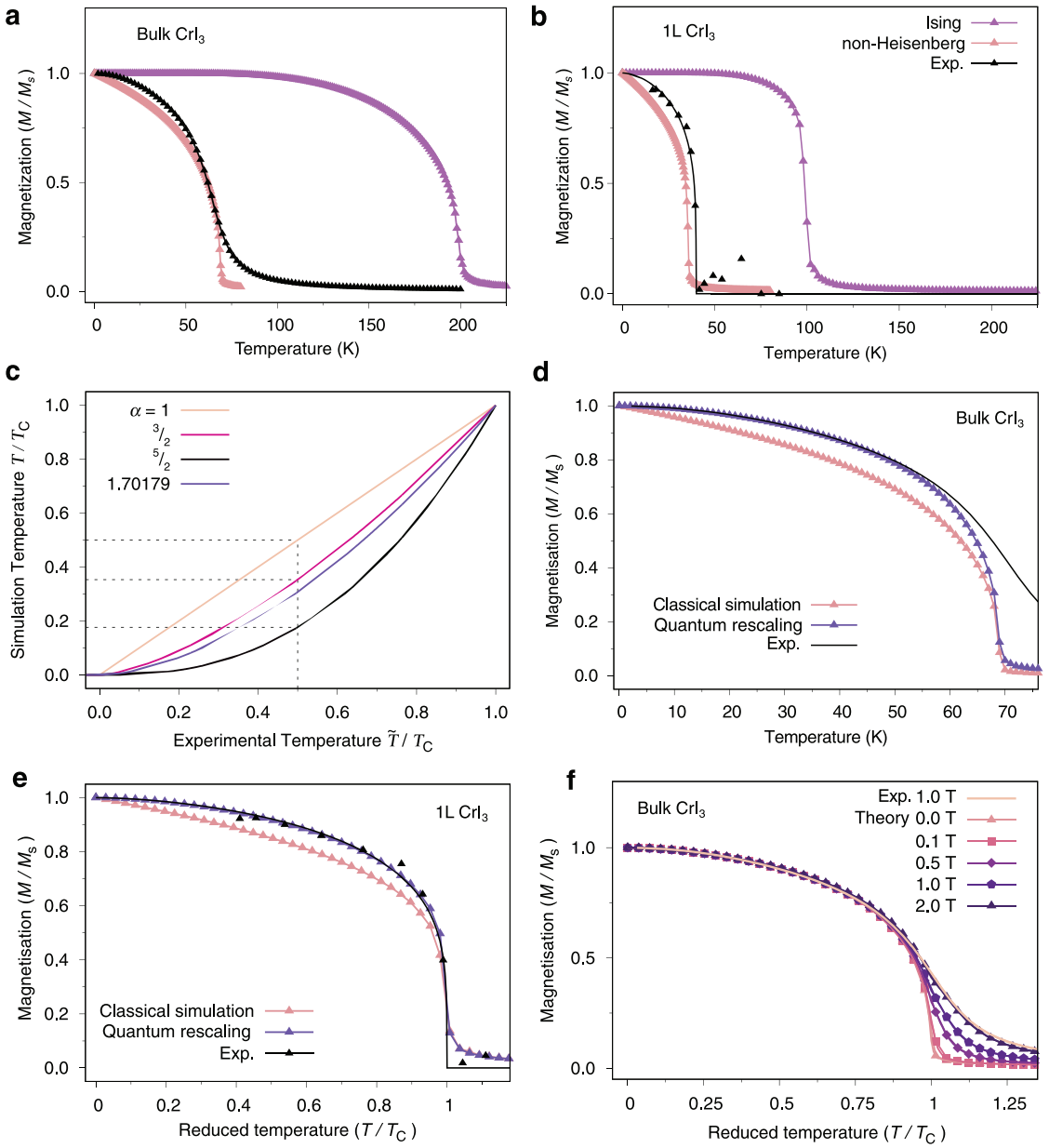

Figure 1. Quantum rescaling corrections. a,b) Comparison of measured and calculated temperature dependent magnetization (M/M_s) of bulk and monolayer (1L) CrI_3, respectively, using Ising and non-Heisenberg models (Equation (1)). In both cases, the Ising model leads to large overestimation of the Curie temperature (T_C) relative to the experiments. Even with the inclusion of biquadratic exchange into the description of the spin interactions, some deviations relative to the experiments are observed at low-temperatures. c) Plot of the effective simulation (spin) temperature against the comparable experimental temperature of the environment for different values of the phenomenological rescaling exponent α. For $\alpha = 1$, the two temperatures are equal and represents the usual situation for a classical Heisenberg magnet. For increasing values of α, the effective spin temperature is reduced due to the quantum nature of the heat bath reducing the spin fluctuations. The value of $\alpha = 1.70179$ extracted from the measured data for bulk CrI_3 is shown for comparative purposes. d) Detailed comparison of the classical non-Heisenberg simulation and the experimental data for bulk CrI_3 at a magnetic field of $B_z = 1.0$ T. The linear behavior of the magnetization at low temperatures is a well-known deficiency of a classical model. Applying quantum rescaling to include the quantum nature of the heat bath gives a quantitative agreement with the experimental data at the low temperature regime. At elevated temperatures, the differences arise due to the presence of an external magnetic field which resulted in values of T_C of 69 K from simulations and 63 K from experiments. e) Magnetization as a function of the reduced temperature (T/T_C) for monolayer CrI_3 comparing classical and quantum rescaling-corrected simulations with the experimental data. The data is plotted normalized to T_c due to the small difference between measured and calculated Curie temperatures to enable a direct comparison of the top of the magnetization curve. The fitted line to the experimental data uses the computed value of $\beta = 0.22 \pm 0.004$ from the classical simulation and assumed temperature rescaling exponent $\alpha = 1.70$ fitted from the bulk experimental data. f) Comparative simulations of the temperature dependent magnetization for bulk CrI_3 in different applied magnetic fields including temperature rescaling and normalized to T_C. The simulations show a sound agreement with the experimental data at temperatures less than T_C, while above T_C the apparent paramagnetic susceptibility is lower in the simulations due to an absence of quantum effects above the Curie temperature.

spin flip occurs. Macroscopically this significantly reduces the average strength of the thermal spin fluctuations within the simulation which we approximate by applying a simple temperature rescaling of the form

$$T_{\text{sim}} = (T_{\text{exp}}/T_{\text{C}})^{1/\alpha} \tag{2}$$

where α is a phenomenological rescaling exponent extracted from the experimental data (Figure 1c). The fitting assumes a simple Curie–Bloch interpolation of the form:

$$m(T) = [1-(T/T_{\text{C}})^{\alpha}]^{\beta} \tag{3}$$

and is seen to fit a wide range of ferromagnetic and antiferromagnetic materials including the current material of interest, CrI_3. Practically our rescaling approach is only applicable over an ensemble average of hundreds of spins as individual scattering events are not directly simulated within our semi-classical method, but effectively introduce the quantum nature of the heat bath within a classical model. Nevertheless, the ability of the classical non-Heisenberg model to quantitatively reproduce the temperature dependent properties of bulk CrI_3 is remarkable. Figure 1d highlights the difference between simulations with and without quantum rescaling corrections for bulk CrI_3. It is clear that the classical nature of the atomistic spin model[39] induced discrepancies with the measured data below T_{C}. As the spins are treated classically using a non-Heisenberg Hamiltonian, which follows the Boltzmann distribution, the curvature of the measured $M(T)$ deviates from the classical behavior due to infinitesimal thermal fluctuations of the spins at the low temperature regime. These fluctuations of the magnetization have a quantum origin that are better represented using quantum statistics within the Bose–Einstein distribution.

By fitting Equation (3) to the bulk experimental data with $\beta_{\text{bulk}} \approx 0.25$ initially extracted from the classical simulation we obtain excellent agreement between the scaled and measured $M(T)$ for $T < T_{\text{C}}$ at $\alpha = 1.70$. For the monolayer data (Figure 1e), we follow the same process as for the bulk, computing $\beta_{\text{1L}} = 0.22$ from first principles and Monte Carlo calculations. Assuming that the Bloch exponent α is independent of dimensionality, we find a sound agreement with the measured data for monolayer CrI_3. The different β values compared to bulk ferromagnets indicate the criticality of the magnetization near the Curie temperature, and are not universal properties of Heisenberg and Ising systems in contrast with previous studies.[32] The Bloch exponent and therefore quantum corrections are sufficient to explain the different shapes of $M(T)$ curves without the need to resort to fundamentally different models, for example Ising, Kitaev, or XY models (Section S4, Supporting Information). We also performed quantitative comparison between simulated and measured data for $M(T)$ at different magnitudes of the magnetic field B_z (Figure 1f). The applied B_z reduces the criticality of the magnetization close to the Curie temperature, and the simulations converge towards the experimental data mainly for temperatures below T_{C} with negligible differences (less than 1%.) Moreover, the field dependence of the magnetization above the Curie point is stronger in the experiments compared to the simulations since we do not take into account quantum rescaling effects above T_{C}. The roughly double amount of B_z in the simulations to reproduce the experimental dependence beyond the Curie point suggests that quantum effects are still important as spin wave excitations or magnons may be present as previously observed in other magnetic materials.[40,41] In reality an externally applied field affects the microscopic spin fluctuations and therefore alters the thermodynamic distribution of spins, for thin magnets it leads to a larger equilibrium magnetization than for the purely classical approach even far above T_{C}.[40]

An outstanding question raised by the experiments is why a macroscopic magnetization or a monodomain exists in a 2D system after zero-field cooling. It is known that magnetic anisotropy overcomes the limit of the Mermin–Wagner theorem by symmetry breaking, but one would ordinarily expect that magnetic domains are stable in the system, particularly in high-anisotropy materials such as CrI_3. To investigate this we simulated the zero-field and field cooling processes for a large square nano-flake of monolayer CrI_3 of dimensions 0.4 μm × 0.4 μm using atomistic spin dynamics (see Section S5, Supporting Information). The system is thermally equilibrated above the Curie temperature and then linearly cooled to 0 K in a simulated time of 2 ns for different values of applied external magnetic field, as shown in **Figure 2** and Movies S1–S3, Supporting Information. From the simulations we extract the time evolution of the spins and the formation of magnetic domains extracting snapshots of the spin configurations during the zero-field cooling process. For zero magnetic field shown in Figure 2a–c we find that the magnetic domains are metastable (Movie S1, Supporting Information) while for a small field of $B_z = 10$ mT the domains are mostly removed during the 2 ns cooling process (Figure 2d–f, Movie S2, Supporting Information). For the zero field cooling the domains persist until the end of the simulation, but show a continuous evolution in time at 0 K showing their metastable nature. As the field increases to 50 mT (Movie S3, Supporting Information) the domains are flushed out with a homogeneous magnetization being observed over the entire simulation area (0.4 μm × 0.4 μm) after 2 ns. Our observations suggest that magnetic domains are not intrinsically stable in CrI_3, which indicates a macroscopic magnetization throughout the surface even in zero-magnetic field. Domains as large as 0.57 μm have been observed (Movie S1, Supporting Information). Moreover, the interplay between metastability and large magnetic anisotropy could give the physical ingredients for the coexistence of different domain wall types in CrI_3. This effect could be intrinsic to 2D vdW magnets with wide implications for device developments and real applications.

Interestingly, the metastability of the domains prevents the wall profiles from reaching a truly ground-state configuration. A projection of the magnetization **M** over the domain walls at 0 K and zero field (Figure 2g) shows that such unstable magnetic domains can be of several types (Figure 2h–k). This is particularly acute near the middle of the sample where quenching leads to a frustrated set of domains and the in-plane direction of the magnetizations rotates repeatedly. This effect is also observed closer to the edge where it is possible to observe a persistent rotation of the in-plane magnetization (Figure 2k) over short lengths of the wall but extending over the entire boundary of the magnetic domains. For the few domain walls that can be stabilized at a specific magnetization direction, we find that the majority of the magnetic domain walls in CrI_3 (around 97%)

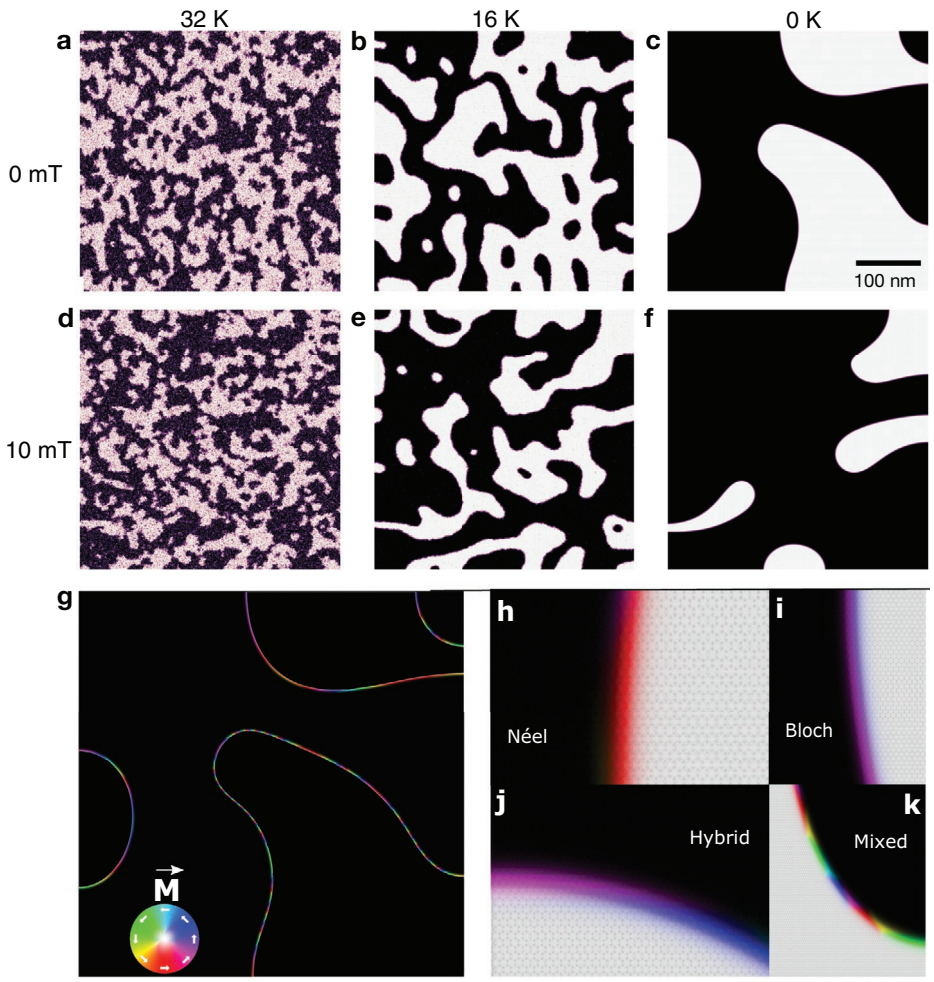

Figure 2. Theory-predicted magnetic domains in monolayer CrI_3. a–f) Magnetic domain configurations obtained during field cooling at 0 mT and 10 mT, respectively. The bright and dark areas at $T \leq 16$ K correspond to spins pointed along the easy-axis in different spin polarizations (e.g., up or down). The purple and mixed colors correspond to different spin orientations either before stabilization of the domains at $T \geq 16$ K, or at the domain walls at $T \leq 16$ K. As the system cools down the magnetic domains coalesce to form a circular shape to minimize the domain wall energy. Domains anti-parallel to the field direction are unstable, and eventually reverse leaving a saturated domain state at low temperatures. g) Analysis of the domain walls from (c) at different parts of the crystals undertaking an in-plane projection of the magnetization $\vec{M}$ according to its color orientation at the domain walls. h–k) A coexistence of several domain wall types is observed through Néel (h), Bloch (i), hybrid (j), and mixed (k) domain walls. A continuous rotation of the spins is observed in the hybrid domains which extends from few tens of Å up to few nanometers.

are Néel-type (Figure 2i) but with some large proportion of a new hybrid type (Figure 2h) with characteristics between Bloch (Figure 2j) and Néel walls. A minor amount of domains, less than 3%, stabilized at Bloch type over the entire system. These domains were obtained from different stochastic realizations of the zero field cooling simulations.

To determine whether such diverse domain walls have additional characteristics in monolayer CrI_3, we project the total magnetization at the wall over in-plane (M_x, M_y) and out-of-plane (M_z) components (**Figure 3**a,c,e). While M_z through Bloch, hybrid and Néel domains does not change appreciably, both M_x and M_y show different behavior characterizing a specific kind of domain wall with its specific spin orientations (Figure 3b,d,f). It is noteworthy that the hybrid domains have a different chirality for the in-plane moments relative to Bloch and Néel with a sizable component along of the y axis as the spins transition from one domain to another (Figure 3c,d and Figure 2h). We can extract the domain wall width δ by fitting the different components of the magnetization (M_x, M_y, M_z) to a standard equation profile of the form:

$$M(r) = \tanh(\pi(r - r_0)/\delta) \tag{4}$$

where r_0 is the domain wall position at a specific orientation (x, y, z). All types of wall have a very narrow domain wall width of around $\delta \approx 3.8$ to 4.8 nm (Figure 3a,c,e). Such small domain walls are typically only seen in permanent magnetic materials due to the exceptionally high magnetic anisotropy.[42] For such materials the magnetic domains are stabilized in a zero-remanence state after zero-field cooling due to the long-ranged dipole–dipole interactions which are also taken into account in our calculations (Section S9, Supporting Information). Nevertheless we find that this is not the case for monolayer CrI_3 which suggests that this material

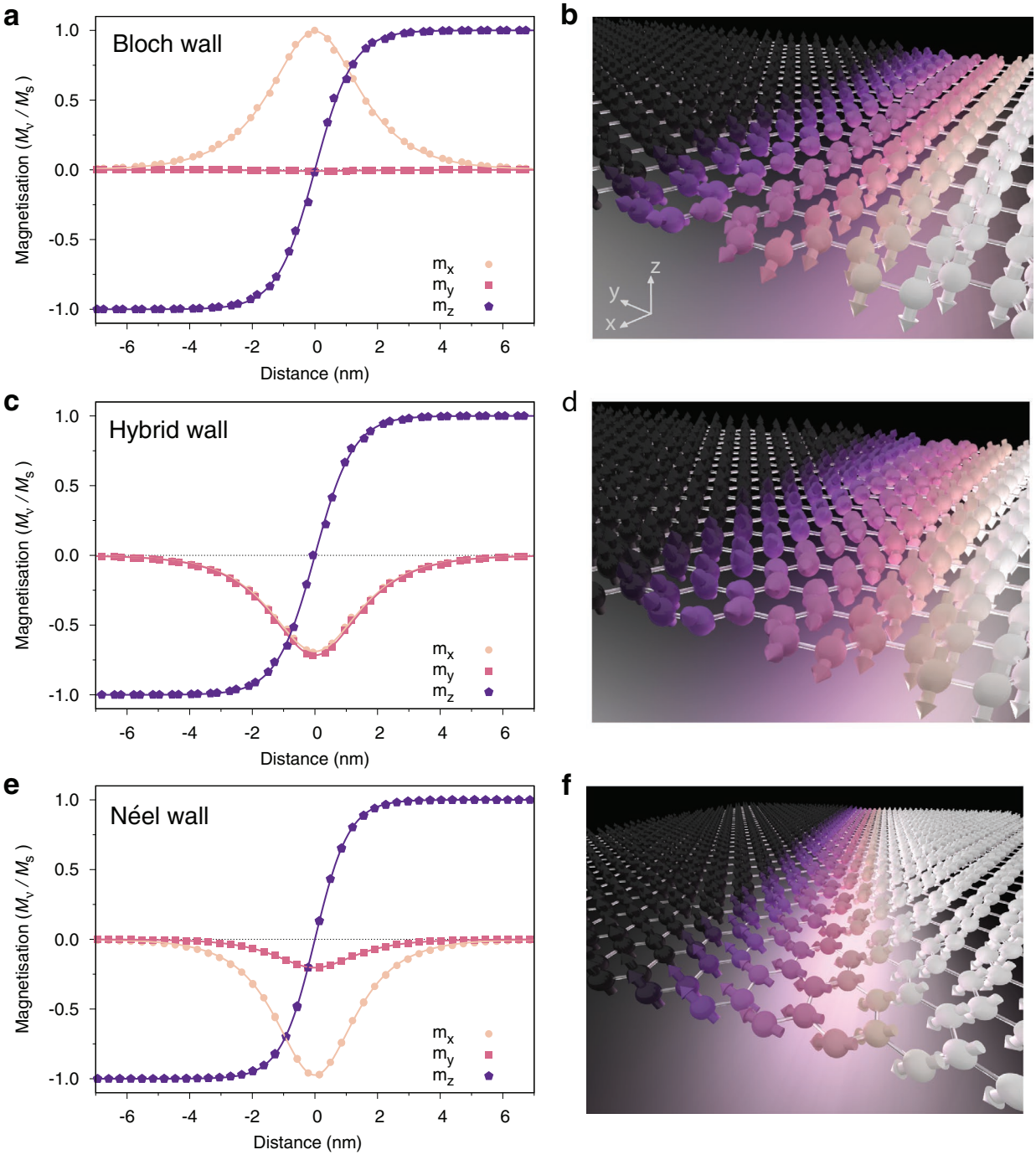

Figure 3. Simulated hybrid domain-walls. Plot of the domain wall profiles for metastable domain walls at $T = 0$ K for two different stochastic realizations in monolayer CrI_3. Three characteristic shapes are seen: a,b) Bloch type, where the in-plane magnetization (M_x, M_y) is parallel to the domain wall. c,d) Hybrid type, where the in-plane magnetization is between Néel and Bloch type and lies at some angle to the wall direction. e,f) Néel–Néel-type where the in-plane magnetization is perpendicular to the domain wall. The schematics in the right show a visualization of the individual spin directions in the domain wall. Note that the different sign of the *x* and *y* components indicates a different domain wall chirality. The out of plane magnetization (M_z) does not show appreciable modifications over the three domains observed. The calculated domain wall width is in the range of 3.8–4.8 nm. Such narrow widths are typically only found in permanent magnets such as L10-FePt nanoparticles or $Nd_2Fe_{14}B$ crystals.[42]

reunites features from a soft-magnet (e.g., easy movement of domain walls, small area hysteresis loop) and a hard-magnet (e.g., relative high magnetocrystalline anisotropy, narrow domain walls).

The variety of domain-walls observed in CrI_3 can be directly related to the magnetic stability of the layer.[42] For magnetic materials with strong uniaxial anisotropy, the equilibrium state is normally reached beyond the field cooling process.[43] Even

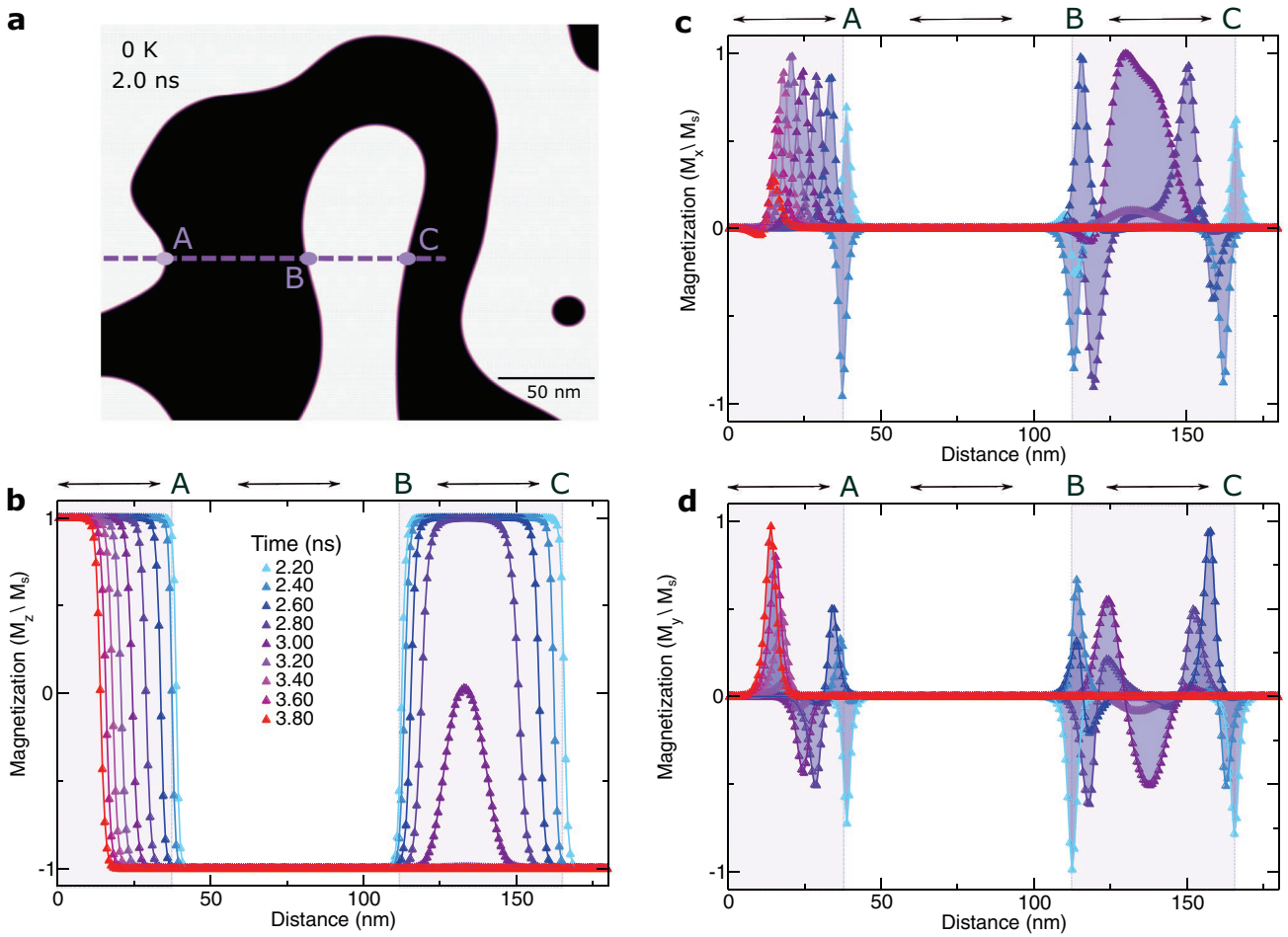

Figure 4. Modeling of spin fluctuations across domains. a) Snapshot of a spin dynamics of monolayer CrI_3 obtained through zero-field cooling down process after 2.00 ns and reaching 0 K. The magnetization along of the easy-axis (M_z) is displayed showing the domain formation. Bright (dark) areas correspond to $M_z = \pm 1$, respectively. A path (dashed line) connecting three points A, B, and C at the boundary between different magnetic domains is showed. b–d) Variations of M_z and the out-of-plane components of the magnetization (M_x, M_y), respectively, along of A–B–C at different times (2.40–3.80 ns) after 0 K is obtained. The shaded areas determine the regions considered along the path.

though no thermal energy would be available at such limit, the spins would still evolve to stabilize the ground-state via the minimization of other contributions of the total energy, for example, exchange, anisotropy. This process can be observed in **Figure 4** for the time-evolution of one of the spin dynamics of monolayer CrI_3 once the system had achieved 0 K within 2.0 ns at zero field. There is a continuous modification of the domain-wall profiles through all components of the magnetization ($M_{x,y,z}$) over time. The variations on M_z across the magnetic domains (Figure 4a,b) tend to be smooth without sudden changes differently to those observed along the in-plane components (Figure 4c,d). For them, several peaks appeared and vanished on a time scale of few tenths of nanoseconds indicating the stochastic nature of the spin-fluctuations in the system. Indeed, we observed such random fluctuations of $M_{x,y}$ even beyond 20 ns which suggest that the system may be intrinsically not a local minimum but rather at a flat energy landscape. We can extract some qualitative information about the magnetic behavior of the domains in CrI_3 regarding stability and domain size using magnetic force microscopy (MFM) experiments (see Section S10, Supporting Information for details). Figures S18 and S19, Supporting Information shows a zero-field cooled CrI_3 thick flake (0.04 μm) with lateral dimensions of approximately 4 μm × 2 μm at 4.2 K where magnetic domains of about 2 μm persist to the base temperature (Figure S19a,b, Supporting Information). Even though the measurements were undertaken at a sample area one order of magnitude larger than that utilized in the simulations (e.g. 0.16 μm^2), the magnetic domains formed in both theory and experiments still keep the same scale relative to the domain size created. This indicates that mostly a monodomain is created over the entire surface as suggested by the theoretical results. Moreover, the topography of the domains extracted from frequency shift profiles (Figure S19f–i, Supporting Information) clearly shows sharp domain walls (e.g., smaller than 20 nm) but the resolution limitation of the MFM technique (50 nm diameter of an average Cr coated MFM tip) prevents the direct comparison with the sub-10 nm prediction extracted from theory. Similar limitation (≈40–60 nm) was also observed in recent measurements using a scanning single-spin magnetometry with a nitrogen-vacancy

(NV) center spin in the tip of an atomic force microscope[44] and a magnetic circular-dichroism technique.[45] This indicates that further development on the experimental side is needed to further validate the simulation results. It is worth mentioning that even though the time-scale used in the spin dynamics spans around 20 ns, it reproduces accurately the domain structure obtained via MFM over a few hours scan process. The images recorded in Figure S19, Supporting Information may be considered as the final magnetic state as several electronic and spin interactions take place. The early stages which determined the magnetic ordering can be extracted from the micromagnetic simulations as a sound agreement is obtained with the recorded MFM images. In addition, atomistic simulations undertake in bulk CrI_3 (Figure S20, Supporting Information) support the picture that magnetic domains are more stable in bulk (Figures S18 and S19, Supporting Information) than in monolayer due to the additional interlayer interactions driven by vdW forces and spin exchange. Thus, the meta-stability of the magnetic domains seems to be more present in the lower dimensionality of single sheets.

The magnetism of 2D materials at the limit of one or few layers is still at its early stages with rich phenomena yet to be explored. The demonstration here of quantum effects in CrI_3 together with its non-Heisenberg character due to higher-order exchange interactions should motivate significant future studies to understand both the mechanism of the computed enhancement of biquadratic interactions and to confirm that such effect may be general to several families of 2D vdW magnets. In addition, the metastability of the magnetic domains in CrI_3 induces a homogeneous magnetization or even a single domain over the entire surface. This behavior associated with the out-of-plane anisotropy and the higher coercivity of CrI_3 indicates a potential magnetic media for perpendicular recording. It is still unclear however which kind of domain motion can be foreseen in such thin layered compound, and how the coexistence of different domain types can affect device architectures. This suggests new routes for magnetic-domain engineering at the atomic limit.

Data Availability

The data that support the findings of this study are available within the paper and its Supporting Information.

Supporting Information

Supporting Information is available from the Wiley Online Library or from the author.

Acknowledgements

R.F.L.E. gratefully acknowledges the financial support of the Engineering and Physical Sciences Research Council (Grant No. EPSRC EP/P022006/1) and the use of the VIKING Cluster, which is a high-performance compute facility provided by the University of York. This work was enabled by code enhancements to the VAMPIRE software implemented under the embedded CSE programme (ecse0709) and (ecse1307) of the ARCHER UK National Supercomputing Service. E.J.G.S. acknowledges computational resources through the UK Materials and Molecular Modelling Hub for access to THOMAS supercluster, which is partially funded by EPSRC (EP/P020194/1); CIRRUS Tier-2 HPC Service (ec131 Cirrus Project) at EPCC (http://www.cirrus.ac.uk) funded by the University of Edinburgh and EPSRC (EP/P020267/1); ARCHER UK National Supercomputing Service (http://www.archer.ac.uk) via Project d429. E.J.G.S. acknowledges the EPSRC Early Career Fellowship (EP/T021578/1) and the University of Edinburgh for funding support. E.N.-M. acknowledges the European Research Council (ERC) under the Horizon 2020 Research and Innovation Programme (ERC StG, grant agreement No. 803092). ENM also acknowledges financial support from the Spanish Ministerio de Ciencia, Innovación y Universidades for financial support from the Ramon y Cajal program (Grant No. RYC2018-024736-I). E.C. acknowledges the financial support from the European Union (ERC AdG Mol-2D 788222 and COST Action MOLSPIN CA15128), the Spanish MICINN (MAT2017-89993-R, RTI2018-098568-A-I, and EQC2018-004888-P co-financed by FEDER and Excellence Unit "María de Maeztu", CEX2019-000919-M), and the Generalitat Valenciana (PO FEDER Program, ref. IDIFEDER/2018/061).

Conflict of Interest

The authors declare no conflict of interest.

Author Contributions

E.J.G.S. conceived the idea and supervised the project. M.A. and D.A.W. performed ab initio and Monte Carlo (MC) simulations under the supervision of E.J.G.S. R.F.L.E. implemented the biquadratic exchange interactions in VAMPIRE, and also undertook MC simulations. S.J. implemented the atomistic dipole-dipole solver to verify the computed domain wall profiles. E.N.M. and S.M.V. fabricated and characterized the samples. I.J.V.-M., W.K., K.S.N. measured the samples using SQUID. E.N.M., S.M.V., E.C. performed the MFM measurements. E.N.M., I.J.V.-M., I.V.G., K.S.N. analyzed the data and contributed to the discussions. E.J.G.S. wrote the paper with inputs from all authors. All authors contributed to this work, read the manuscript, discussed the results, and agreed to the contents of the manuscript.

Keywords

2D magnets, biquadratic exchange, CrI_3, magnetic domains, metastable domains

[1] L. de Jongh, *Magnetic Properties of Layered Transition Metal Compounds*, Springer, Dordrecht, The Netherlands **2012**.
[2] B. Huang, G. Clark, E. Navarro-Moratalla, D. R. Klein, R. Cheng, K. L. Seyler, D. Zhong, E. Schmidgall, M. A. McGuire, D. H. Cobden, W. Yao, D. Xiao, P. Jarillo-Herrero, X. Xu, *Nature* **2017**, *546*, 270.
[3] C. Gong, L. Li, Z. Li, H. Ji, A. Stern, Y. Xia, T. Cao, W. Bao, C. Wang, Y. Wang, Z. Q. Qiu, R. J. Cava, S. G. Louie, J. Xia, X. Zhang, *Nature* **2017**, *546*, 265.
[4] T. Song, X. Cai, M. W.-Y. Tu, X. Zhang, B. Huang, N. P. Wilson, K. L. Seyler, L. Zhu, T. Taniguchi, K. Watanabe, M. A. McGuire, D. H. Cobden, D. Xiao, W. Yao, X. Xu, *Science* **2018**, *360*, 1214.
[5] D. R. Klein, D. MacNeill, J. L. Lado, D. Soriano, E. Navarro-Moratalla, K. Watanabe, T. Taniguchi, S. Manni, P. Canfield, J. Fernández-Rossier, P. Jarillo-Herrero, *Science* **2018**, *360*, 1218.

[6] D. Ghazaryan, M. T. Greenaway, Z. Wang, V. H. Guarochico-Moreira, I. J. Vera-Marun, J. Yin, Y. Liao, S. V. Morozov, O. Kristanovski, A. I. Lichtenstein, M. I. Katsnelson, F. Withers, A. Mishchenko, L. Eaves, A. K. Geim, K. S. Novoselov, A. Misra, *Nat. Electron.* **2018**, *1*, 344.

[7] Z. Wang, I. Gutiérrez-Lezama, N. Ubrig, M. Kroner, M. Gibertini, T. Taniguchi, K. Watanabe, A. Imamoğlu, E. Giannini, A. F. Morpurgo, *Nat. Commun.* **2018**, *9*, 2516.

[8] Z. Fei, B. Huang, P. Malinowski, W. Wang, T. Song, J. Sanchez, W. Yao, D. Xiao, X. Zhu, A. F. May, W. Wu, D. H. Cobden, J.-H. Chu, X. Xu, *Nat. Mater.* **2018**, *17*, 778.

[9] K. L. Seyler, D. Zhong, D. R. Klein, S. Gao, X. Zhang, B. Huang, E. Navarro-Moratalla, L. Yang, D. H. Cobden, M. A. McGuire, W. Yao, D. Xiao, P. Jarillo-Herrero, X. Xu, *Nat. Phys.* **2018**, *14*, 277.

[10] Y. Tian, M. J. Gray, H. Ji, R. J. Cava, K. S. Burch, *2D Mater.* **2016**, *3*, 025035.

[11] Z. Guguchia, A. Kerelsky, D. Edelberg, S. Banerjee, F. von Rohr, D. Scullion, M. Augustin, M. Scully, D. A. Rhodes, Z. Shermadini, H. Luetkens, A. Shengelaya, C. Baines, E. Morenzoni, A. Amato, J. C. Hone, R. Khasanov, S. J. L. Billinge, E. Santos, A. N. Pasupathy, Y. J. Uemura, *Sci. Adv.* **2018**, *4*, eaat3672.

[12] R. Skomski, *Simple Models of Magnetism*, Oxford Graduate Texts, Oxford University Press, Oxford, UK **2008**.

[13] J. C. Slonczewski, *Phys. Rev. Lett.* **1991**, *67*, 3172.

[14] M. Bode, M. Heide, K. von Bergmann, P. Ferriani, S. Heinze, G. Bihlmayer, A. Kubetzka, O. Pietzsch, S. Blügel, R. Wiesendanger, *Nature* **2007**, *447*, 190.

[15] S. Rohart, A. Thiaville, *Phys. Rev. B* **2013**, *88*, 184422.

[16] L. Chen, J.-H. Chung, B. Gao, T. Chen, M. B. Stone, A. I. Kolesnikov, Q. Huang, P. Dai, *Phys. Rev. X* **2018**, *8*, 041028.

[17] W. Jin, H. H. Kim, Z. Ye, S. Li, P. Rezaie, F. Diaz, S. Siddiq, E. Wauer, B. Yang, C. Li, S. Tian, K. Sun, H. Lei, A. W. Tsen, L. Zhao, R. He, *Nat. Commun.* **2018**, *9*, 5122.

[18] I. Lee, F. G. Utermohlen, D. Weber, K. Hwang, C. Zhang, J. van Tol, J. E. Goldberger, N. Trivedi, P. C. Hammel, *Phys. Rev. Lett.* **2020**, *124*, 017201.

[19] A. Kartsev, M. Augustin, R. F. L. Evans, K. S. Novoselov, E. J. G. Santos, arXiv:2006.04891, **2020**.

[20] J. Hellsvik, M. Balestieri, T. Usui, A. Stroppa, A. Bergman, L. Bergqvist, D. Prabhakaran, O. Eriksson, S. Picozzi, T. Kimura, J. Lorenzana, *Phys. Rev. B* **2014**, *90*, 014437.

[21] N. S. Fedorova, C. Ederer, N. A. Spaldin, A. Scaramucci, *Phys. Rev. B* **2015**, *91*, 165122.

[22] P. Novák, I. Chaplygin, G. Seifert, S. Gemming, R. Laskowski, *Comput. Mater. Sci.* **2008**, *44*, 79.

[23] A. Kitaev, *Ann. Phys. (Amsterdam, Neth.)* **2006**, *321*, 2.

[24] C. Xu, J. Feng, H. Xiang, L. Bellaiche, *npj Comput. Mater.* **2018**, *4*, 57.

[25] É. L. Nagaev, *Sov. Phys.-Usp.* **1982**, *25*, 31.

[26] A. L. Wysocki, K. D. Belashchenko, V. P. Antropov, *Nat. Phys.* **2011**, *7*, 485.

[27] E. A. Harris, J. Owen, *Phys. Rev. Lett.* **1963**, *11*, 9.

[28] A. M. Turner, F. Wang, A. Vishwanath, *Phys. Rev. B* **2009**, *80*, 224504.

[29] H.-F. Zhu, H.-Y. Cao, Y. Xie, Y.-S. Hou, S. Chen, H. Xiang, X.-G. Gong, *Phys. Rev. B* **2016**, *93*, 024511.

[30] M. Hoffmann, S. Blügel, *Phys. Rev. B* **2020**, *101*, 024418.

[31] R. F. L. Evans, W. J. Fan, P. Chureemart, T. A. Ostler, M. O. A. Ellis, R. W. Chantrell, *J. Phys.: Condens. Matter* **2014**, *26*, 103202.

[32] Y. Liu, C. Petrovic, *Phys. Rev. B* **2018**, *97*, 014420.

[33] G. T. Lin, X. Luo, F. C. Chen, J. Yan, J. J. Gao, Y. Sun, W. Tong, P. Tong, W. J. Lu, Z. G. Sheng, W. H. Song, X. B. Zhu, Y. P. Sun, *Appl. Phys. Lett.* **2018**, *112*, 072405.

[34] Y. K. Fu, Y. Sun, X. Luo, *J. Appl. Phys.* **2019**, *125*, 053901.

[35] J. L. Lado, J. Fernández-Rossier, *2D Mater.* **2017**, *4*, 035002.

[36] H. H. Kim, B. Yang, S. Li, S. Jiang, C. Jin, Z. Tao, G. Nichols, F. Sfigakis, S. Zhong, C. Li, S. Tian, D. G. Cory, G.-X. Miao, J. Shan, K. F. Mak, H. Lei, K. Sun, L. Zhao, A. W. Tsen, *Proc. Natl. Acad. Sci. USA* **2019**, *116*, 11131.

[37] S. Li, Z. Ye, X. Luo, G. Ye, H. H. Kim, B. Yang, S. Tian, C. Li, H. Lei, A. W. Tsen, K. Sun, R. He, L. Zhao, *Phys. Rev. X* **2020**, *10*, 011075.

[38] R. F. L. Evans, U. Atxitia, R. W. Chantrell, *Phys. Rev. B* **2015**, *91*, 144425.

[39] M. D. Kuz'min, *Phys. Rev. Lett.* **2005**, *94*, 107204.

[40] H. J. Qin, K. Zakeri, A. Ernst, J. Kirschner, *Phys. Rev. Lett.* **2017**, *118*, 127203.

[41] X. Tao, D. P. Landau, T. C. Schulthess, G. M. Stocks, *Phys. Rev. Lett.* **2005**, *95*, 087207.

[42] *Magnetic Domains: The Analysis of Magnetic Microstructures*, Springer, Berlin/Heidelberg, Germany **1998**.

[43] D. Wulferding, H. Kim, I. Yang, J. Jeong, K. Barros, Y. Kato, I. Martin, O. E. Ayala-Valenzuela, M. Lee, H. C. Choi, F. Ronning, L. Civale, R. E. Baumbach, E. D. Bauer, J. D. Thompson, R. Movshovich, J. Kim, *Sci. Rep.* **2017**, *7*, 46296.

[44] L. Thiel, Z. Wang, M. A. Tschudin, D. Rohner, I. Gutiérrez-Lezama, N. Ubrig, M. Gibertini, E. Giannini, A. F. Morpurgo, P. Maletinsky, *Science* **2019**, *364*, 973.

[45] D. Zhong, K. L. Seyler, X. Linpeng, N. P. Wilson, T. Taniguchi, K. Watanabe, M. A. McGuire, K.-M. C. Fu, D. Xiao, W. Yao, X. Xu, *Nat. Nanotechnol.* **2020**, *15*, 187.